Effects of lattice geometry and interaction range on polaron dynamics

J. P. Hague,[1] P. E. Kornilovitch,[2] A. S. Alexandrov,[1] and J. H. Samson[1]

[1]*Department of Physics, Loughborough University, Loughborough, LE11 3TU, United Kingdom*
[2]*Hewlett-Packard Company, 1000 NE Circle Blvd., Corvallis, Oregon 97330, USA*

We study the effects of lattice type on polaron dynamics using a continuous-time quantum Monte Carlo approach. Holstein and screened Fröhlich polarons are simulated on a number of different Bravais lattices. The effective mass, isotope coefficients, ground-state energy and energy spectra, phonon numbers, and density of states are calculated. In addition, the results are compared with weak- and strong-coupling perturbation theory. For the Holstein polaron, it is found that the crossover between weak- and strong-coupling results becomes sharper as the coordination number is increased. In higher dimensions, polarons are much less mobile at strong coupling, with more phonons contributing to the polaron. The total energy decreases monotonically with coupling. Spectral properties of the polaron depend on the lattice type considered, with the dimensionality contributing to the shape and the coordination number to the bandwidth. As the range of the electron-phonon interaction is increased, the coordination number becomes less important, with the dimensionality taking the leading role.

PACS number(s): 71.38.$-$k, 02.70.Ss, 74.20.$-$z

I. INTRODUCTION

Interest in the role of electron-phonon (e-ph) interactions and polaron dynamics in contemporary materials has recently gone through a large revival. Electron-phonon interactions have been shown to be relevant in the cuprate superconductors through isotope substitution experiments,[1] recent high-resolution angle-resolved photoemission,[2] and a number of earlier optical[3,4] and neutron-scattering[5] spectroscopies. In the colossal magnetoresistance manganites, isotope substitution also shows a significant effect on the physical properties.[6] It has been suggested that the long-range Fröhlich e-ph interaction is relevant in cuprates and manganites at any doping because of poor screening,[7] although the spatial extent of the interactions is still part of an ongoing discussion.[8]

The polaron problem has been actively researched for a long time (for a review see Refs. 9 and 10). For weak electron-phonon coupling $\lambda \ll 1$ in the adiabatic limit $\hbar\omega/E_F \ll 1$, Migdal theory describes electron dynamics.[11] With increasing strength of interaction and increasing phonon frequency ω finite bandwidth[12,13] and vertex corrections[14] become important. The neglect of vertex corrections in the Migdal approximation breaks down entirely at $\lambda \sim 1$ for any value of the adiabatic ratio $\hbar\omega/E_F$ because the bandwidth is narrowed and the Fermi energy is renormalized down exponentially. As a result, the effective parameter $\lambda\hbar\omega/E_F$ becomes large.[15] In the strong-coupling limit $\lambda \gg 1$, a canonical Lang-Firsov (LF) transformation can be used to determine the properties of the small polaron.[16] The effective mass does not diverge at a critical coupling but instead increases exponentially. No general solution to the polaron problem exists for all values of the coupling constant, except in the infinite-dimensional limit where dynamical mean-field theory (DMFT) can be applied.[17] It is the enormous differences between weak- and strong-coupling limits and adiabatic and antiadiabatic limits which make the polaron problem in the intermediate λ regime difficult to study analytically and numerically.

Several methods exist for the numerical simulation of the polaron problem at intermediate λ. They include exact diagonalization,[18] advanced variational methods[19] (effects of dimensionality are also discussed), conventional discrete-time path integral quantum Monte Carlo (QMC) algorithms[20,21] as well as the newer density matrix renormalization group[22] (DMRG), continuous-time QMC,[23,24] LF QMC,[25,26] and diagrammatic QMC.[27,28] The methods vary in accuracy and versatility but none can provide all the polaron properties of interest in the entire space of model parameters. For instance, exact diagonalizations suffer from the necessary truncation of the phonon Hilbert space, especially at strong couplings and low phonon frequencies (even then, the total Hilbert space is huge, reducing the number of sites and leading to poor momentum resolution), DMRG cannot easily handle long-range interactions, diagrammatic QMC and exact diagonalization are inconvenient in calculating the density of states, path-integral QMC slows down at small frequencies, and so on. In numerical analysis of polaron models, a complex approach is needed where each method is employed to calculate what it does best.

In this paper we use one of these methods, the continuous-time path-integral quantum Monte Carlo algorithm (CTQMC) to investigate the effects of lattice geometry on the properties of the polaron from weak to strong coupling. This algorithm was developed previously by one of us[23] and was based on the analytical integration of phonons introduced by Feynman[29] and on an earlier numerical implementation in discrete time by De Raedt and Lagendijk.[21] CTQMC introduced two critical improvements. Firstly, formulation in continuous imaginary time eliminated errors caused by the Trotter slicing and made the method numerically exact for any strength of electron-phonon interaction. Secondly, introduction of twisted boundary conditions in imaginary time[23,30] enabled calculation of polaron effective masses, spectra, and even densities of states. Although the method is not ideal [it slows down at low phonon frequency because of the condition on inverse temperature $\beta = 1/k_B T$
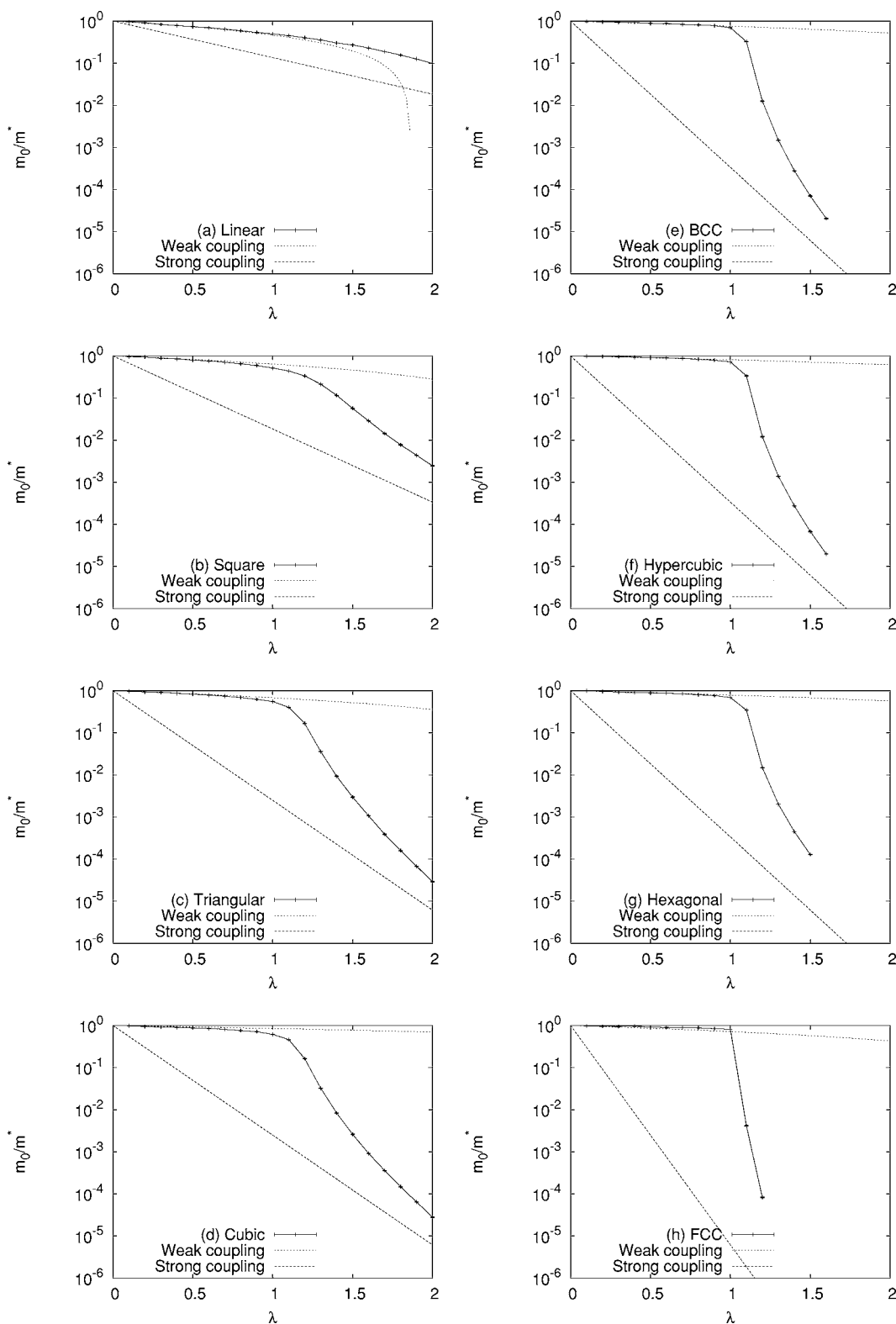
FIG. 1. Inverse effective mass for the Holstein polaron as a function of coupling λ on (a) linear, (b) square, (c) triangular, (d) cubic, (e) body-center-cubic, (f) hypercubic ($d=4$), (g) hexagonal, and (h) face-center-cubic lattices, and $\bar{\omega}=1$. Also shown are the weak and strong coupling asymptotes as calculated in Sec. III. Note that the effective masses of triangular and cubic lattices are almost equivalent for $\lambda > 1$ (both lattices having $z=6$). Also the bcc, hexagonal, and hypercubic lattices ($z=8$) have almost identical curves. It can also be seen that the coincidence occurs well before the approach to the strong coupling asymptote, indicating that the coordination number is very important to physical properties for most values of the coupling. Increased coordination number leads to more mobile polarons at weak coupling and more localized polarons for strong coupling with a very fast crossover between the two behaviors. Error bars show the standard error of the points computed using a blocking scheme.
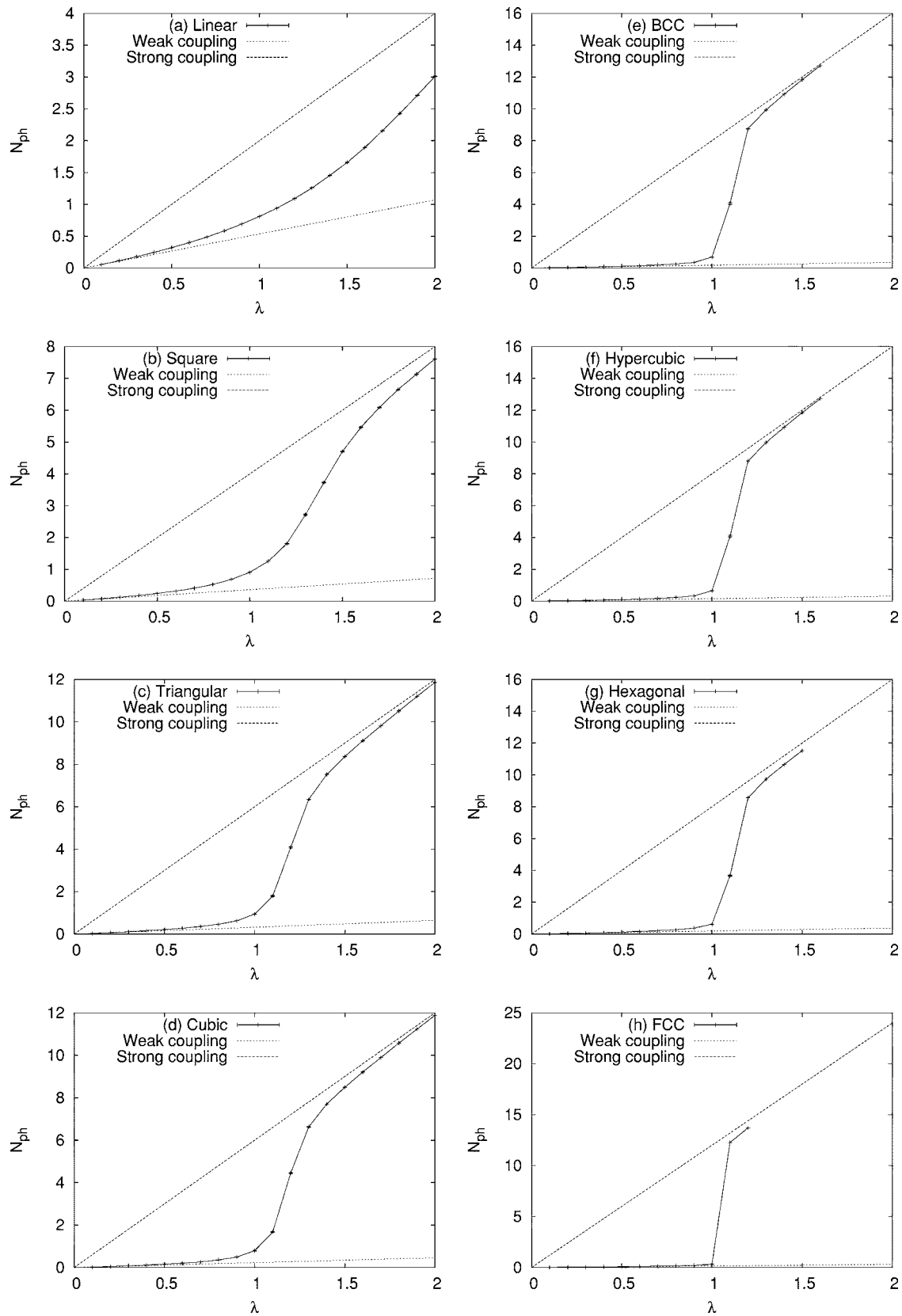
FIG. 2. Number of phonons associated with the Holstein polaron for increasing coupling with $\bar{\omega}=1$. For most couplings, the number of phonons is closely related to the exponent of the effective mass. This is expected in the very strong coupling limit where $m_0/m^*=\exp(-\gamma N_{ph})$, and the continuation of this behavior to lower λ values is of interest. Again, the speed of the crossover and the value of λ at which the number of phonons reaches the strong coupling saturation value depends on the coordination number, not on the dimensionality.
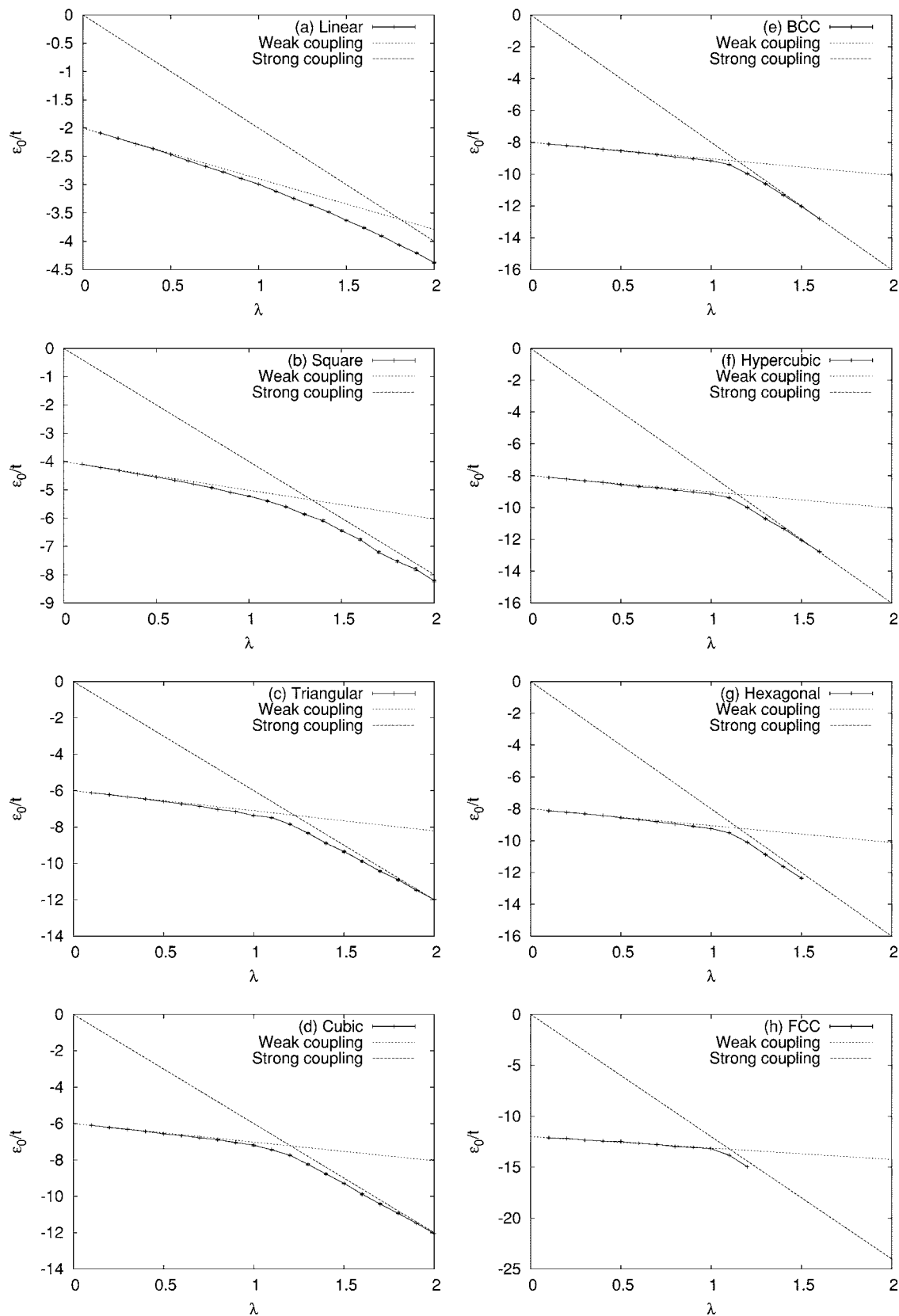
FIG. 3. Total energy of the Holstein polaron for increasing coupling λ with $\bar{\omega}=1$. Note that the crossover from weak to strong coupling behavior is very fast for this quantity on the triangular and cubic lattices, but is much slower for the square lattice. In general, the speed of the crossover is quicker for larger coordination number. The curve lies below the strong coupling asymptote for variational reasons and also lies below the weak-coupling result.
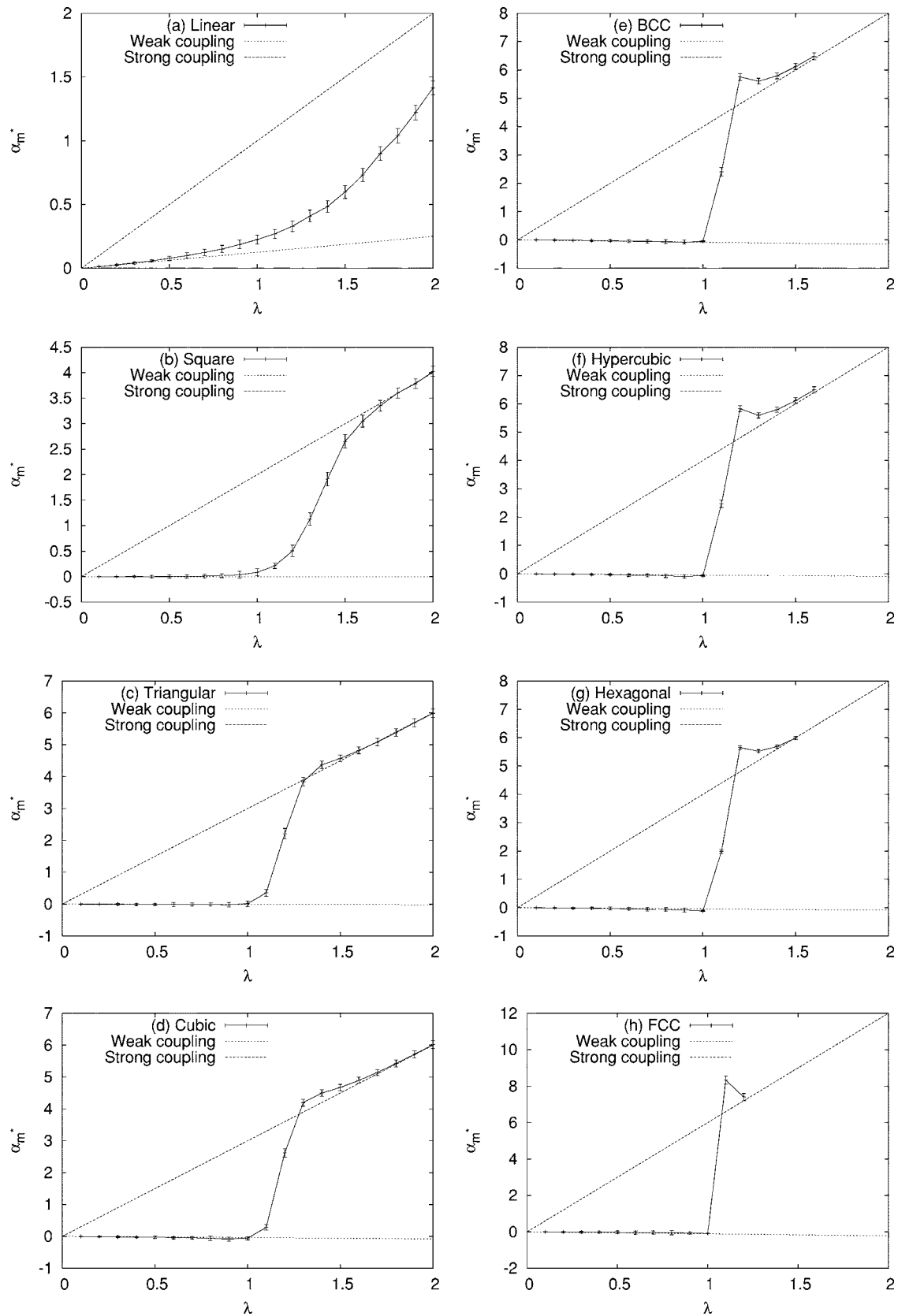
FIG. 4. Mass isotope coefficient of the Holstein polaron with increasing coupling and $\bar{\omega}=1$. At small λ, the α_{m^*} is negative and small, so the effective mass decreases with increased ion mass. Alternatively, the strong coupling behavior shows a clear increase of polaron mass with ion mass. There is an anomalous bump in the isotope coefficient for lattices with $z > 6$.
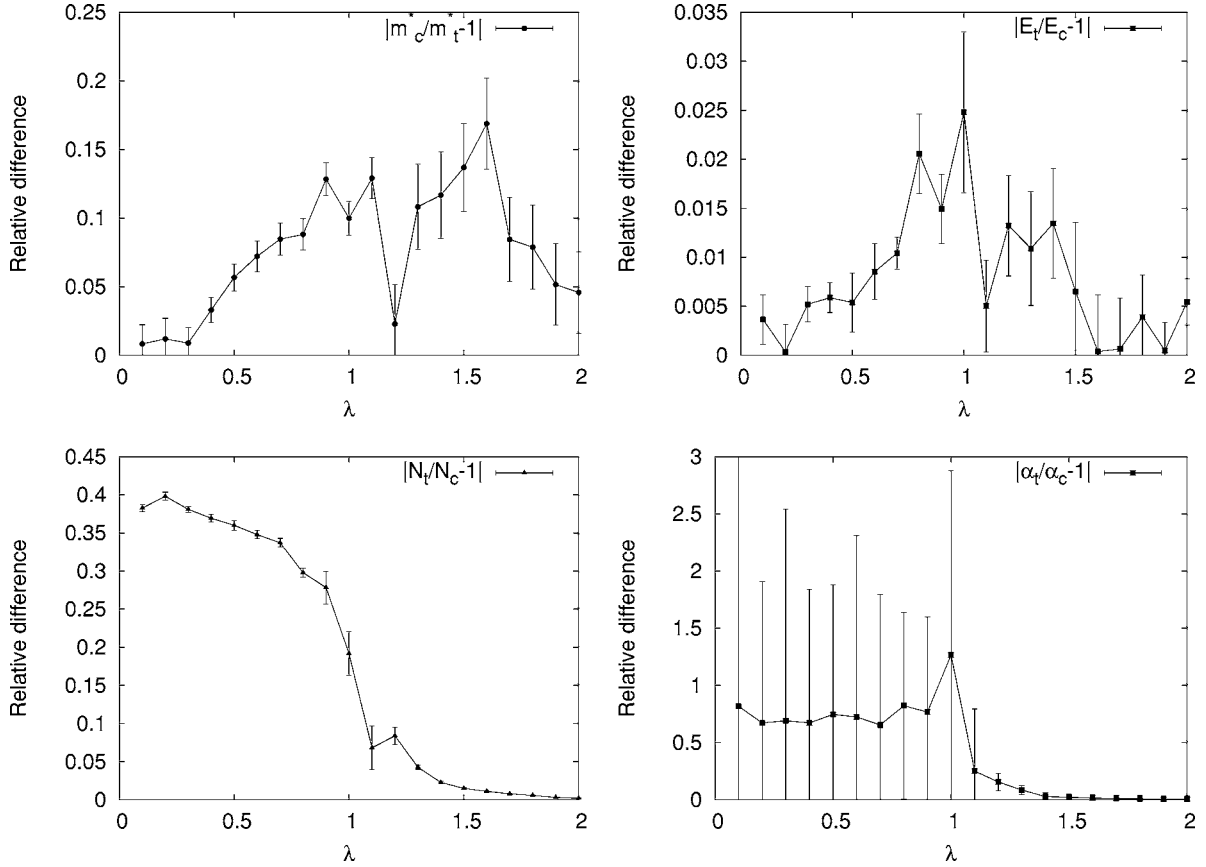
FIG. 5. Relative differences of physical observables on the cubic and triangular lattices. The total energy is identical to within 2% on the triangular and cubic lattices, followed by the effective mass, which is within 20% on both lattices. All quantities agree well for $\lambda > 1$.

$\gg (\hbar \omega)^{-1}$ and suffers from a sign problem at small coupling and large polaron momentum] it is quite versatile. In particular, it has enabled accurate analysis of models with long-range electron-phonon interactions[24,31] and a model with anisotropic electron hopping.[32] In addition, it is currently the only method that can provide numerically *exact* polaron densities of states[23] and isotope exponents.[24,33] We note that the variational approach of Trugman *et al.* has been used to compute the mass isotope effect of the bipolaron, and presumably such a method could be used to compute the isotope exponent for the polaron.[19]

In this paper, we develop the algorithm further. Because it is formulated in real space it is ideally suited for analyzing more complex lattices than the conventional linear, square, and cubic Bravais lattices. All that is needed is a redefined set of nearest-neighbor hops (or kinks) by which the QMC process moves the polaron path through the space. We will analyze and compare several Bravais lattices: linear, square and triangular in $d=2$, simple cubic, face-center-cubic (fcc), hexagonal and body-center-cubic (bcc) in $d=3$, and simple hypercubic in $d=4$. To our knowledge, this is the first investigation of this kind in the polaron literature. In Sec. II, we introduce a model of electron-phonon interactions and briefly describe the method applied in this work. In Sec. III we describe the limiting behavior of the polaron problem on different lattices. In Sec. IV, we apply CTQMC to the lattice Holstein polaron and calculate dynamical quantities such as the effective mass, polaron dispersion and density of states.

The effects of changing the length scale of the interaction are discussed in Sec. V. Finally we discuss the relevance of these results in Sec. VI.

II. MODEL AND METHOD

We restrict the model to have only one electron Wannier state $|\mathbf{n}\rangle$ and one phonon degree of freedom $\xi_{\mathbf{m}}$ per lattice unit cell. The unit cells are numbered by the indices $\mathbf{n}$ or $\mathbf{m}$. The electron hopping is assumed to be isotropic and between the nearest neighbors only. The phonon subsystem is a set of independent oscillators with frequency ω and mass M. In the real space representation the Hamiltonian reads

$$H = H_e + H_{\mathrm{ph}} + H_{e\text{-}\mathrm{ph}}, \tag{1}$$

with

$$H_e = -t \sum_{\langle \mathbf{nn'} \rangle} c_{\mathbf{n'}}^{\dagger} c_{\mathbf{n}}, \tag{2}$$

$$H_{\mathrm{ph}} = \frac{1}{2M} \sum_{\mathbf{m}} \hat{P}_{\mathbf{m}}^2 + \frac{M\omega^2}{2} \sum_{\mathbf{m}} \xi_{\mathbf{m}}^2, \tag{3}$$

$$H_{e\text{-}\mathrm{ph}} = -\sum_{\mathbf{nm}} f_{\mathbf{m}}(\mathbf{n}) c_{\mathbf{n}}^{\dagger} c_{\mathbf{n}} \xi_{\mathbf{m}}. \tag{4}$$

Here t is the hopping amplitude, $\langle \mathbf{nn'} \rangle$ denote pairs of nearest neighbors, and $\hat{P}_{\mathbf{m}} = -i\hbar \partial / \partial \xi_{\mathbf{m}}$ is the ion momentum op-
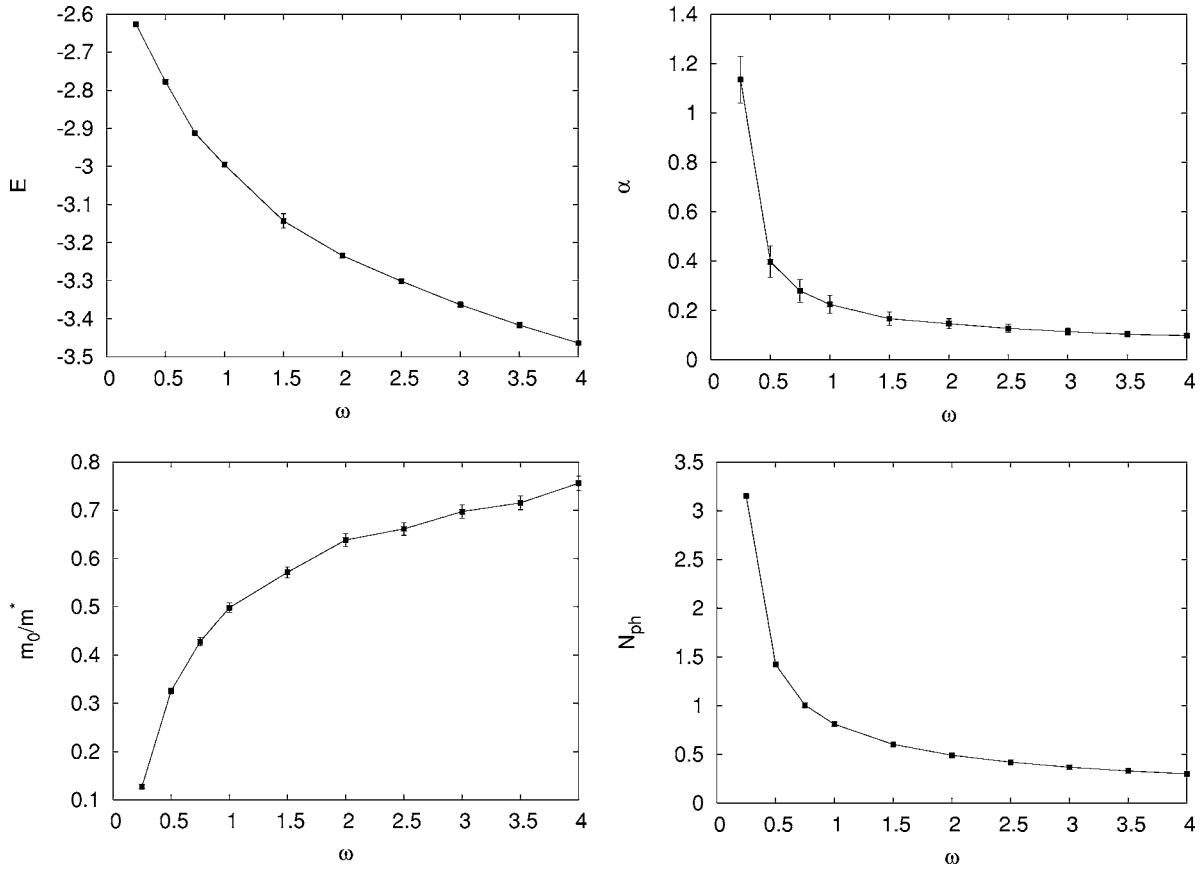
FIG. 6. Variation of physical observables with phonon frequency, $\bar{\omega}$ on a linear chain with $\lambda = 1$. The physics remains qualitatively similar throughout, with no fast crossover or transition in any property.

erator. The spin indices are absent because the system contains only one electron.

The form of electron-phonon interaction is specified via the *force* function $f_{\mathbf{m}}(\mathbf{n})$. The latter is defined as the force with which an electron in state $|\mathbf{n}\rangle$ interacts with the ion degree of freedom $\xi_{\mathbf{m}}$. In this paper, we consider two types of the force function: (i) the short-range Holstein interaction $f_{\mathbf{m}}(\mathbf{n}) = \kappa \delta_{\mathbf{nm}}$[34] and (ii) a screened discrete Fröhlich interaction

$$f_{\mathbf{m}}(\mathbf{n}) = \frac{\kappa}{[(\mathbf{m}-\mathbf{n})^2+1]^{3/2}} \exp\left(-\frac{|\mathbf{m}-\mathbf{n}|}{R_{sc}}\right). \quad (5)$$

In $d=2$ (or $d=1$), it describes the screened *isotropic* Coulomb interaction of an electron with *linearly* polarized lattice distortions. The distortions are polarized perpendicular to the plane (chain) of the electron motion, and their equilibrium positions are shifted perpendicular to the plane (chain) by one lattice period. In Eq. (5), κ is a constant and R_{sc} is the screening radius in units of the lattice vector. Note that the Holstein model is recovered for $R_{sc}=0$ and the lattice Fröhlich model for $R_{sc} \rightarrow \infty$. The interaction (5) was introduced in Ref. 24 to model hole-phonon interaction in doped cuprates. Its various limiting cases were studied in Refs. 31, 32, 35, and 36.

The focus of this paper is the effects of the lattice geometry on the polaron properties. Each lattice is characterized

by its coordination number z and the bare electron dispersion $E_{\mathbf{k}} = -tN^{-1}\Sigma_{\langle \mathbf{n},\mathbf{n}' \rangle} \exp[i\mathbf{k}\cdot(\mathbf{n}-\mathbf{n}')]$. (For example, for the triangular lattice, $E_{\mathbf{k}} = -2t\{\cos k_x a + \cos[\frac{1}{2}k_x + (\sqrt{3}/2)k_y]a + \cos[\frac{1}{2}k_x - (\sqrt{3}/2)k_y]a\}$.) In particular, we will be interested in comparing Bravais lattices with equal z but different dimensionality, d. We will analyze the cases $z=2$ (linear chain), $z=4$ (square in $d=2$), $z=6$ (triangular in $d=2$ and simple cubic in $d=3$), $z=8$ (body-centered cubic in $d=3$, simple hexagonal in $d=3$ ($t_\parallel = t_\perp$), and hyper cubic in $d=4$), and $z=12$ (face-center-cubic in $d=3$). Note that the minimum bare electron energy is $-zt$ for all these lattices.

The dimensionless coupling constant of the electron-phonon interaction λ is defined as follows:

$$\lambda = \frac{1}{2M\omega^2 zt} \sum_{\mathbf{m}} f_{\mathbf{m}}^2(0). \quad (6)$$

This coupling constant is the ratio of the polaron energy in the atomic limit (i.e., at $t=0$) to the kinetic energy of the free electron zt. It is also convenient to introduce the dimensionless phonon frequency $\bar{\omega} \equiv \hbar\omega/t$, the dimensionless inverse temperature $\bar{\beta} \equiv \beta t$, and the dimensionless force $\bar{f}_{\mathbf{m}}(\mathbf{n}) \equiv \kappa^{-1}f_{\mathbf{m}}(\mathbf{n})$.

The CTQMC method employed here has been described in detail elsewhere[23,24] so here we give a quick overview of the algorithm. The initial step is to determine the effective
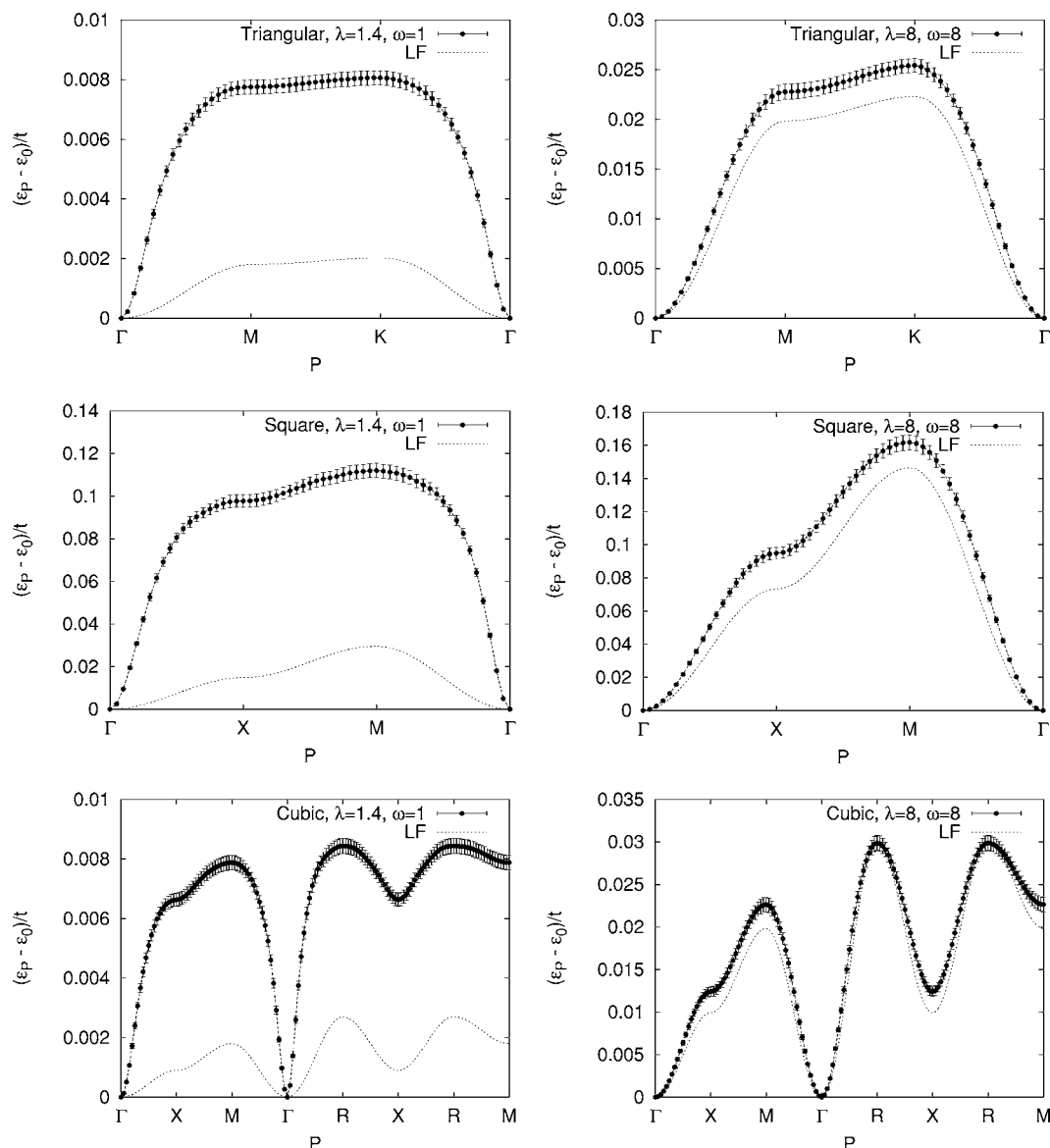
FIG. 7. Dispersion of the Holstein polaron in the near-adiabatic ($\bar{\omega}=1$, $\lambda=1.4$) and antiadiabatic ($\bar{\omega}=8$, $\lambda=8$) regimes. Also shown is the result from the Lang-Firsov approximation. The band width remains dependent on the coordination number, with the polaron spectra of the cubic and triangular lattices having similar width. Alternatively, the shape of the dispersion is clearly related to the dimensionality. As expected, the Lang-Firsov dispersion is quite accurate in the antiadiabatic limit and fails in the adiabatic limit.

electron (polaron) action that results when the phonon degrees of freedom have been integrated out analytically. The action is a functional of the polaron path in imaginary time $\mathbf{r}(\tau)$ and is given by the following double integral:

$$A[\mathbf{r}(\tau)] = \frac{z\lambda\bar{\omega}}{2\Phi_0(0,0)} \int_0^{\bar{\beta}} \int_0^{\bar{\beta}} d\tau d\tau' e^{-\bar{\omega}\bar{\beta}/2}(e^{\bar{\omega}(\bar{\beta}/2-|\tau-\tau'|)}$$

$$+ e^{-\bar{\omega}(\bar{\beta}/2-|\tau-\tau'|)})\Phi_0[\mathbf{r}(\tau),\mathbf{r}(\tau')]$$

$$+ \frac{z\lambda\bar{\omega}}{\Phi_0(0,0)} \int_0^{\bar{\beta}} \int_0^{\bar{\beta}} d\tau d\tau' e^{-\bar{\omega}\tau} e^{-\bar{\omega}(\bar{\beta}-\tau')}$$

$$\times \{\Phi_{\Delta\mathbf{r}}[\mathbf{r}(\tau),\mathbf{r}(\tau')] - \Phi_0[\mathbf{r}(\tau),\mathbf{r}(\tau')]\}, \quad (7)$$

$$\Phi_{\Delta\mathbf{r}}[\mathbf{r}(\tau),\mathbf{r}(\tau')] = \sum_{\mathbf{m}} \bar{f}_{\mathbf{m}}[\mathbf{r}(\tau)]\bar{f}_{\mathbf{m}+\Delta\mathbf{r}}[\mathbf{r}(\tau')], \quad (8)$$

where the vector $\Delta\mathbf{r}=\mathbf{r}(\beta)-\mathbf{r}(0)$ is the difference between the end points of the polaron path. These expressions are valid when the condition $\exp(\bar{\beta}\bar{\omega}) \geqslant 1$ is satisfied. From this starting point, the polaron is simulated using the Metropolis Monte Carlo method. The electron path is continuous in time with hopping events (or kinks) introduced or removed from the path with each Monte Carlo step. From this ensemble, various physical properties may be computed. The ground state polaron energy is

$$\epsilon_0 = -\lim_{\beta \to \infty} \left[\left\langle \frac{\partial A}{\partial \beta} \right\rangle - \frac{1}{\beta} \left\langle \sum_s N_s \right\rangle \right], \quad (9)$$

where N_s is the number of kinks of type s, and angular brackets denote ensemble averaging. The number of phonons is given by

$$N_{ph} = -\lim_{\beta \to \infty} \frac{1}{\beta} \left\langle \frac{\partial A}{\partial \bar{\omega}} \bigg|_{\lambda \bar{\omega}} \right\rangle, \quad (10)$$

where the derivative is taken keeping $\lambda \bar{\omega}$ constant. The polaron band energy spectrum can be computed from

$$\epsilon_{\mathbf{k}} - \epsilon_0 = -\lim_{\beta \to \infty} \frac{1}{\beta} \ln\langle \cos(\mathbf{k} \cdot \Delta \mathbf{r}) \rangle, \quad (11)$$

where $\mathbf{k}$ is the quasimomentum. By expanding this expression in small $\mathbf{k}$, the ith component of the inverse effective mass is obtained as

$$\frac{1}{m_i^*} = \lim_{\beta \to \infty} \frac{1}{\beta \hbar^2} \langle (\Delta r_i)^2 \rangle. \quad (12)$$

Thus the inverse effective mass is the diffusion coefficient of the polaron path in the limit of the infinitely long "diffusion time" β. Finally, the mass isotope coefficient, $\alpha_{m_i^*} = d \ln m_i^* / d \ln M$, is calculated as follows:

$$\alpha_{m_i^*} = \lim_{\beta \to \infty} \frac{\bar{\omega}}{2} \frac{1}{\langle (\Delta r_i)^2 \rangle} \left[\left\langle (\Delta r_i)^2 \frac{\partial A}{\partial \bar{\omega}} \bigg|_\lambda \right\rangle - \langle (\Delta r_i)^2 \rangle \right.$$
$$\left. \times \left\langle \frac{\partial A}{\partial \bar{\omega}} \bigg|_\lambda \right\rangle \right]. \quad (13)$$

Here the action derivatives must be taken at constant λ. $\alpha_{m_i^*}$ and effective mass averaged over dimensions are related to the critical temperature isotope coefficient, $\alpha = -d \ln T_c / d \ln M$, of a (bi)polaronic superconductor as

$$\alpha = \alpha_{m^*} \left(1 - \frac{m_0/m^*}{\lambda - \mu_c} \right), \quad (14)$$

where μ_c is the Coulomb pseudopotential.[15,37]

Several of the lattices studied here are not bipartite, and observables will quantitatively change with sign of t. In this paper t is always taken to be positive (corresponding to s orbitals, etc.) Negative t would lead to a sign problem, since the probability of the update is proportional to t. One could probably proceed by mapping the negative t problem onto a modified positive t problem with long range hopping. We leave such a study for a future publication.

III. LIMITING BEHAVIOR

In this section, we discuss limiting behaviors for the polaron problem to demonstrate the physical differences between the two limits. The results presented here can also be used to check the accuracy of the QMC algorithm, and are compared with the numerical results in the next section.

A. Weak coupling

The weak-coupling behavior can be computed using a simple second-order perturbation theory. In such a theory, the polaron dispersion is given by[38]

$$\epsilon_{\mathbf{k}}^{(2)} = E_{\mathbf{k}} - \frac{z\lambda \bar{\omega} t^2}{\sum_{\mathbf{m}} f_{\mathbf{m}}^2(0)} \frac{1}{N} \sum_{\mathbf{q}} \frac{|f_{\mathbf{q}}|^2}{W(\mathbf{k}, \mathbf{q})}, \quad (15)$$

$$W(\mathbf{k}, \mathbf{q}) = E_{\mathbf{k}-\mathbf{q}} + \hbar\omega - E_{\mathbf{k}}, \quad (16)$$

$$f_{\mathbf{q}} = \sum_{\mathbf{m}} f_{\mathbf{m}}(0) e^{-i\mathbf{q} \cdot \mathbf{m}}, \quad (17)$$

where N is the number of unit cells. Thus the ground-state polaron energy (at $\mathbf{k}=0$) is $\epsilon_0^{(2)} = -t[z + \lambda \Gamma_{\epsilon_0}(\bar{\omega})]$, which defines a dimensionless coefficient Γ_{E_0}. A second derivative of Eq. (15) yields the effective mass

$$\frac{1}{m_i^{*(2)}} = \frac{1}{\hbar^2} \frac{\partial^2 \epsilon_{\mathbf{k}}}{\partial k_i^2} \bigg|_{\mathbf{k}=0} = \frac{1}{m_{0i}}$$
$$- \frac{z\lambda \bar{\omega} t^2}{\hbar^2 N} \sum_{\mathbf{q}} \frac{|f_{\mathbf{q}}|^2}{\sum_{\mathbf{m}} f_{\mathbf{m}}^2(0)} \frac{2W_i'^2 - W_i'' W}{W^3(\mathbf{k}, \mathbf{q})} \equiv \frac{1 - \lambda \Gamma_{m_i^*}(\bar{\omega})}{m_{0i}}, \quad (18)$$

with $W_i' = \partial W / \partial k_i$, etc. In calculating the coefficients $\Gamma_{m_i^*}$ one should take into account that the expression for the bare effective mass changes with lattice type $m_{0i}^{-1} = 2a^2 t / \hbar^2$ for the hypercubic, face-center-cubic, and body-center-cubic lattices, but $m_{0i}^{-1} = 3a^2 t / \hbar^2$ for the triangular lattice. The bare masses are not isotropic on the hexagonal lattice, with in plane $m_{0xy}^{-1} = 3a^2 t / \hbar^2$ and out of plane $m_{0z}^{-1} = 2a^2 t / \hbar^2$, so a little care has to be taken in the following. The mass isotope coefficient is defined as

$$\alpha_{m_i^*}^{(2)} = \frac{\partial \ln(m_i^*)}{\partial \ln(M)} = \frac{\bar{\omega}}{2(m_{0i}/m_i^*)} \frac{\partial}{\partial \bar{\omega}} \left(\frac{m_{0i}}{m_i^*} \right). \quad (19)$$

Substituting here Eq. (18) one obtains to leading order in λ

$$\alpha_{m_i^*}^{(2)} = -\lambda \frac{\bar{\omega}}{2} \frac{\partial \Gamma_{m_i^*}(\bar{\omega})}{\partial \bar{\omega}} \equiv \lambda \Gamma_{\alpha_{m_i^*}}(\bar{\omega}). \quad (20)$$

Finally, the number of phonons associated with the polaron in the ground state is

$$N_{ph}^{(2)} = \frac{z\lambda \bar{\omega} t^2}{\sum_{\mathbf{m}} f_{\mathbf{m}}^2(0)} \frac{1}{N} \sum_{\mathbf{q}} \frac{|f_{\mathbf{q}}|^2}{W^2(0, \mathbf{q})} \equiv \lambda \Gamma_{N_{ph}}(\bar{\omega}). \quad (21)$$

The resulting weak-coupling coefficients Γ can be computed by integrating over $\mathbf{q}$ in the Brillouin zone. For the Holstein interaction at $\bar{\omega}=1$, Γ are given in Table I. Note that for all the lattices considered, $\Gamma_{m_i^*}$ and $\Gamma_{\alpha_{m_i^*}}$ are identical in all directions, so only one value is presented.

B. Strong coupling

For very strong coupling, the electron becomes very heavy and almost localized, since the act of hopping from

TABLE I. Coefficients of the weak coupling behavior for $\bar{\omega}=1$ and the Holstein interaction computed by numerical integration in Eqs. (15)–(21). Note that the mass isotope coefficient in $d>1$ has a small negative value.

Lattice	Γ_{m^*}	Γ_{ϵ_0}	$\Gamma_{N_{ph}}$	$\Gamma_{\alpha_{m^*}}$
Linear	0.5366(6)	0.8944(4)	0.5355(9)	0.12523(0)
Square	0.3610(7)	1.0161(0)	0.3610(4)	−0.00031(3)
Triangular	0.3216(8)	1.1062(2)	0.3217(2)	−0.00903(0)
Cubic	0.1533(6)	1.0229(7)	0.2300(1)	−0.04022(1)
bcc	0.2411(2)	1.0378(8)	0.1808(8)	−0.07974(4)
Hypercubic ($d=4$)	0.1591(5)	1.0168(6)	0.1591(6)	−0.04533(4)
Hexagonal	0.2170(3)	1.0536(0)	0.1928(2)	−0.04461(3)
fcc	0.2856(0)	1.1220(6)	0.1564(8)	−0.11021(3)

one site to another by relaxing the local lattice and then distorting the lattice on a neighboring site is very unfavorable. The energy of the resulting small polaron is given as $E_p=-\lambda zt$. As the effective coupling is reduced, other terms due to hopping become relevant. The expansion about the atomic limit in the hopping parameter (which is small compared to the polaron energy) may be determined through a canonical LF transformation. For nearest neighbor isotropic hopping the strong coupling polaron band dispersion is then given by[15]

$$\epsilon_{\mathbf{k}} = -zt\lambda + e^{-\gamma z\lambda/\bar{\omega}}E_{\mathbf{k}} + O(t/\lambda), \qquad (22)$$

$$\gamma = 1 - \frac{\sum_{\mathbf{m}} f_{\mathbf{m}}(0)f_{\mathbf{m}}(\mathbf{b})}{\sum_{\mathbf{m}} f_{\mathbf{m}}^2(0)}, \qquad (23)$$

where $\mathbf{b}$ is a nearest-neighbor lattice vector (it does not matter which one). Clearly γ varies with interaction and lattice type. For the Holstein interaction ($R_{sc}=0$), which is purely site local, $\gamma=1$. For the lattice Fröhlich potential ($R_{sc}=\infty$) on a square lattice, $\gamma=0.292582$, and for the triangular lattice, $\gamma=0.197577$. Such a polaron is *much* lighter than the Holstein polaron. For the screened Fröhlich interaction with $R_{sc}=1$, the triangular lattice has $\gamma=0.710852$ and the square lattice, $\gamma=0.730176$. The effective mass is computed as before, using the dispersion from Eq. (22)

$$\frac{m_0}{m^*} \approx \exp\left(-\frac{z\gamma\lambda}{\bar{\omega}}\right) \qquad (24)$$

and the isotope exponent is

$$\alpha_{m^*} \approx \frac{\gamma\lambda z}{2\bar{\omega}}. \qquad (25)$$

The number of phonons is calculated directly from $\langle H_{ph}\rangle$, which happens to have exactly half the magnitude of $\langle H_{e\text{-}ph}\rangle$, so

$$N_{ph} \approx -\frac{\epsilon_0}{\hbar\omega} = \frac{z\lambda}{\bar{\omega}}. \qquad (26)$$

The remainder of this paper will concern simulations of the polaron problem using the CTQMC. The numerical results will be discussed with relation to the weak- and strong-coupling limits.

IV. THE HOLSTEIN POLARON

A. Ground state properties from weak to strong coupling

The main difficulty in studying the polaron problem is the intermediate coupling regime. For $\lambda\sim1$, it is necessary to rely on numerical results. In this section, we present ground-state properties of the polaron. These may be determined from CTQMC with no sign problem.

In Fig. 1, we show the computed inverse effective mass in the regime between weak and strong coupling. Also shown on the graphs are the weak and strong coupling results. Panels are as follows: (a) linear ($z=2$), (b) square ($z=4$), (c) triangular ($z=6$), (d) simple cubic ($z=6$), (e) body-center cubic ($z=8$), (f) hypercubic ($d=4$, $z=8$), (g) hexagonal ($z=8$), and (h) face-center cubic ($z=12$), with the same order of increasing coordination number followed for all the graphs in this section. The first two panels are the results for the linear and square lattices, which were presented first in Ref. 23. The linear lattice has the lowest coordination number of all lattices computed here, and as such has the slowest crossover between weak and strong coupling behavior. The inverse mass diverges from the weak-coupling asymptote at couplings $\lambda\sim1$, but the approach to the strong-coupling asymptote is very slow. The crossover is still slow for the square lattice. In contrast, the change between the limiting behaviors is much faster for the triangular lattice, with much larger effective masses in the strong-coupling limit. The strong coupling result depends only on the number of nearest neighbors z. As such, strong coupling results for lattices with identical z have very similar profiles. For example, comparison with the cubic lattice, which also has $z=6$, suggests that z is the defining quantity for the $\lambda>1$ curve, with only the weak-coupling behavior dependent on the lattice type (we have already seen how the strong-coupling limit of the effective mass is exponentially dependent on z in Sec. III B). For lattices with even larger coordination number, this trend continues. For instance, the strong-coupling behavior of the polaron on the bcc lattice with $z=8$ corresponds well to that of the hypercubic lattice in $d=4$ and the hexagonal lattice. Increasing z to 12 (fcc lattice) shows an even sharper transition between weak- and strong-coupling behavior. It should be noted that in our calculation the strong-coupling asymptote of the effective mass depends exponentially on z. We note that in the results from the DMFT with $z\to\infty$ presented in Ref. 17, the ratio $\lambda/\bar{\omega}$ is kept constant as λ is changed, so the phonon frequency is continuously increased and the $\lambda\to\infty$ results correspond to the attractive Hubbard model and are not directly comparable with our results. The computation of m_0/m^* is limited by its magnitude, since small m_0/m^* means high effective mass and rare hopping, so the ensemble has to be sampled for a long time to get good statistics. The curve is truncated at weaker λ for lattices with large coordination number to take account of this problem.

In Fig. 2, the number of phonons in the polaron cloud is displayed. Again, a series of different lattices has been considered. For most couplings, the number of phonons is closely related to the exponent of the effective mass. For small electron-phonon coupling, the polaron cloud is virtually empty. The rate of increase, and the time taken to cross over from weak- to strong-coupling behavior is highly dependent on the lattice type considered. For example, on a square lattice, the phonon number is not saturated to the strong coupling limit until $\lambda \sim 2$, in contrast to the $z=6$ triangular and cubic lattices, which saturate at $\lambda \sim 1.5$. For increasing z the saturation value of λ decreases, with saturation at $\lambda \sim 1$ for the $z=12$ fcc lattice. It is instrumental to consider the ratio $N_{ph}/\ln(m_0/m^*)$ as a measure of the departure from strong coupling.

The total energy is displayed in Fig. 3. The energy decreases monotonically with increased coupling for all lattices. The larger the coordination number, the quicker the crossover between weak- and strong-coupling results. The curve lies below the strong coupling limit for variational reasons, and also lies below the weak-coupling line. It should be noted that, for higher coordination numbers at intermediate coupling, it is necessary to increase the total warmup period. This is due to a metastable state corresponding to a path with no kinks, with single kinks created and then immediately destroyed. The metastable state has the properties of the strong-coupling (atomic) limit. Once two kinks are created (which can take several thousand steps), the system drops out of the metastable state into the lower energy minimum, and the correct form for the total energy is found. Such a metastable state has been discussed in Ref. 39. To speed up the computation, the path is started with several kinks inserted randomly. In this way, the metastable state is avoided.

The mass isotope coefficient α_{m^*} is shown in Fig. 4. Note that for $\bar{\omega}=1$, most lattices have a small negative isotope coefficient for small λ. At couplings $\lambda \sim 1$, the sign of the isotope coefficient flips. For lattices with high coordination number, the curve overshoots the strong-coupling limit, before converging on the asymptote.

In order to determine the extent to which the cubic and triangular lattices are similar, Fig. 5 shows the relative differences of physical observables on the cubic and triangular lattices. The total energy is identical to within 2% on the triangular and cubic lattices, followed by the effective mass, which is within 20% on both lattices. All quantities agree well for $\lambda > 1$.

Finally, we demonstrate that there is no qualitative change of the physics with phonon frequency. Figure 6 shows the variation of physical observables as the phonon frequency is reduced. This has been carried out on a linear chain, so that the low omega regime can be reached with the QMC solver. The physics remains qualitatively similar throughout, with no fast crossover or transition in any property.

B. Excited states

In this section we compute the excitation spectrum and density of states for the polaron gas. The density of states could be used to determine thermodynamic and transport
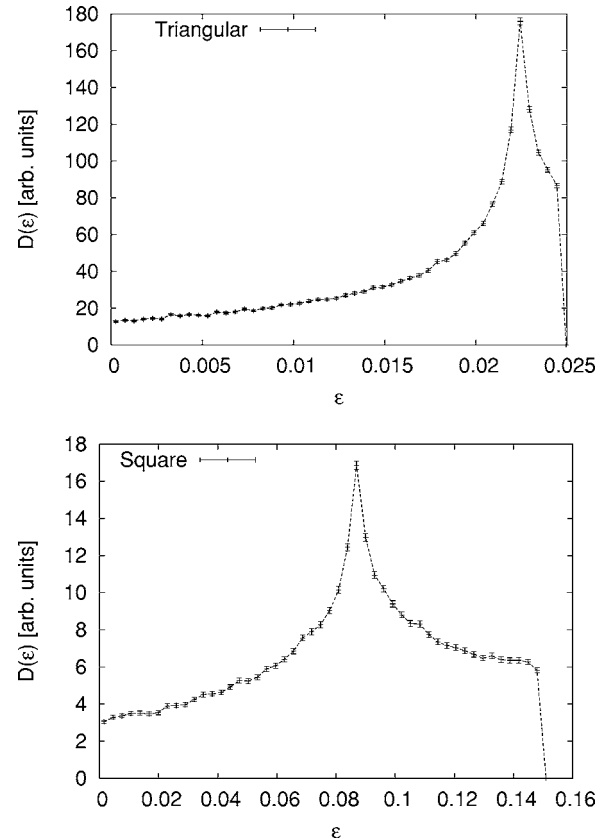

FIG. 8. Density of states for the Holstein interaction in the antiadiabatic limit ($\lambda=8$ and $\bar{\omega}=8$). Again, the effect of dimension can be seen in the shape of the DOS, with the logarithmic divergence (van Hove singularity) clearly visible for both lattices, while the band width is most affected by the coordination number.

properties of the free polaron gas in a similar way to the Sommerfeld theory of metals, although some care should be taken in 1D, where there are no polarons at half filling.[25] In most materials, it is expected that the density of polarons is sufficiently low to avoid such a breakdown of the polaron picture.

The dispersion of the Holstein polaron in the near-adiabatic ($\bar{\omega}=1$, $\lambda=1.4$) and antiadiabatic ($\bar{\omega}=8$, $\lambda=8$) regimes is shown in Fig. 7 for the square, cubic and triangular lattices. Also shown is the result from the LF transformation [Eq. (22)]. Polarons on triangular and cubic lattices are not very mobile in either regime, with the coordination number clearly playing a major role in the bandwidth. Alternatively, the shape of the dispersion is strongly determined by the lattice dimensionality.

Figure 8 shows the density of states (DOS), $D(\epsilon) = \sum_{k} \delta(\epsilon - \epsilon_{k})/N$ for the Holstein polaron in the antiadiabatic limit ($\lambda=8$ and $\bar{\omega}=8$). Again, the effect of dimension can be seen in the shape of the DOS, with the logarithmic divergence (van Hove singularity) clearly visible for both lattices, while the band width is clearly determined by the coordination number (see Ref. 23 for the shape of the DOS of the cubic lattice, which has a completely different form).
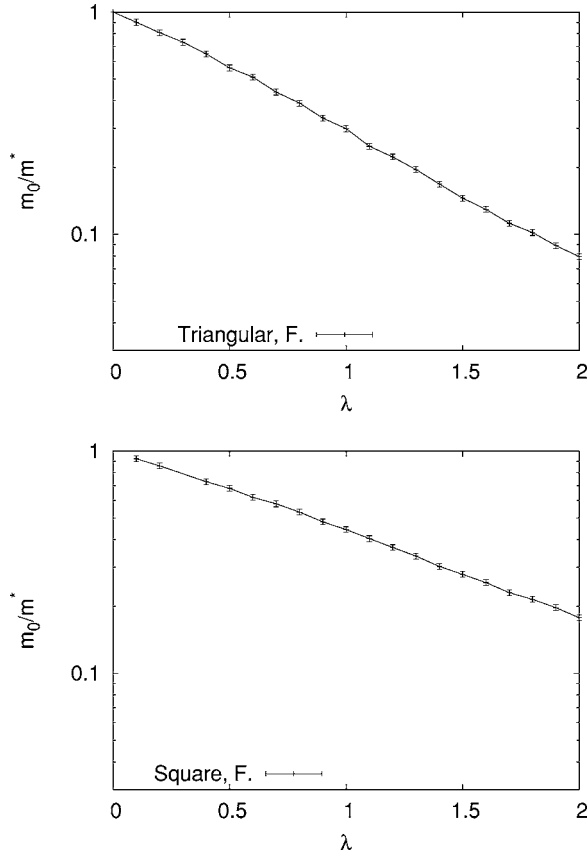
FIG. 9. Inverse mass for the Fröhlich polaron with $\bar{\omega}=1$ ($R_{sc} \rightarrow \infty$). Note that the polaron is far more mobile than in the Holstein case. The results for the two lattices are very similar, indicating that in the case of long range interactions, the dimensionality of the lattice plays a much more important role in the polaron dynamics, with the specific form of the lattice unimportant.

FIG. 10. Dispersion for a screened Fröhlich polaron with $R_{sc}=1$, $\lambda=8$ and $\bar{\omega}=8$. The bandwidth is much larger than in the case of the Holstein interaction. The Lang-Firsov result is also shown (light dotted line). It can be seen that the bandwidths of the triangular and square lattices have the same order of magnitude as the screening radius is increased.

V. EFFECTS OF SCREENING

An important question about polaron properties also involves the effects of screening on the electron-phonon interaction. Unscreened e-ph interactions make polarons very mobile,[7,31] which leads to strong effects even on the qualitative physical properties of the polaron gas. In this section, only the triangular and square lattices are considered.

In Fig. 9, the inverse effective mass for the Fröhlich interaction is plotted. The first point to note is that while the inverse mass in the strong coupling limit depended strongly on the coordination number in the Holstein model, this is no longer true for the Fröhlich polaron. In terms of the way the polaron is formed, the phonon cloud is spread out over several lattice sites. This reduces the dependence on lattice type.

The computation of the energy spectrum is limited by the bandwidth. For very large polaron energies $\epsilon_\mathbf{k} > k_B T$, there is a sign problem introduced by the average of a cosine term [Eq. (11)]. This means that the spectrum can only be computed effectively for small bandwidths. This is not the case for the pure Fröhlich polaron, which is significantly more mobile than the Holstein polaron. In order to circumvent this problem and obtain some information about long range potentials, the screened Fröhlich interaction with $R_{sc}=1$ is used,
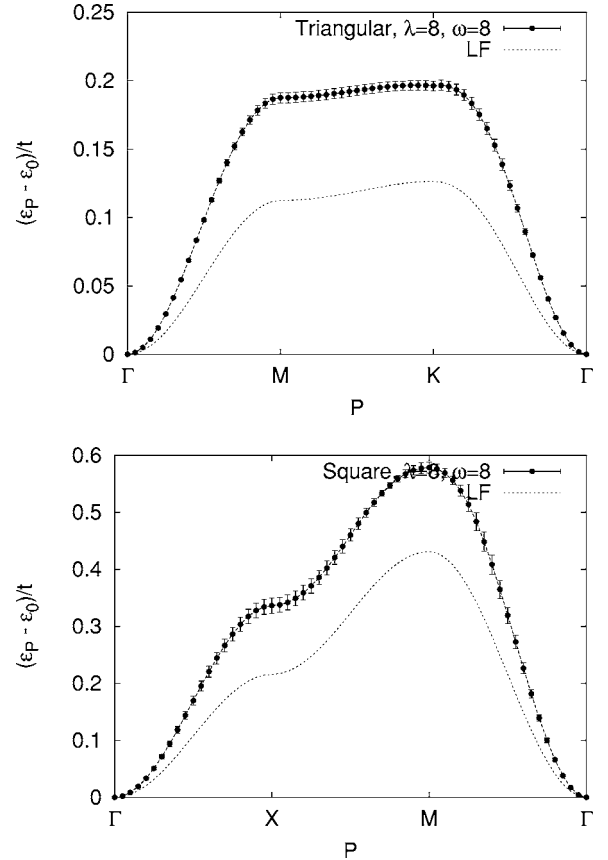
which has some properties of both the Holstein and Fröhlich polarons.

The band structure and density of states (DOS) of the screened Fröhlich polaron are shown in Figs. 10 and 11, respectively. Even for such a small screening length, the effect on the spectrum is dramatic. Again, the shape is given by the lattice type, but now, while the triangular polaron is less mobile than the square polaron, the ratio of bandwidths is much closer to unity than for the Holstein polaron. This is a little surprising, since in this case the polaron extends over very few lattice spacings but the effects of lattice are essentially annulled.

Finally to determine how the relative bandwidths become similar in the Fröhlich polarons on the triangular and square lattices, Fig. 12 shows the evolution of the ratio of the effective bandwidths as the screening length R_{sc} is increased in the near adiabatic limit. The ratio of the bandwidths converges to a constant value ~ 1 with increased screening length, indicating that the effect of the lattice type is essentially washed out for long range potentials.

VI. SUMMARY

We have studied the effects of lattice type on polaron dynamics using a continuous time quantum Monte Carlo
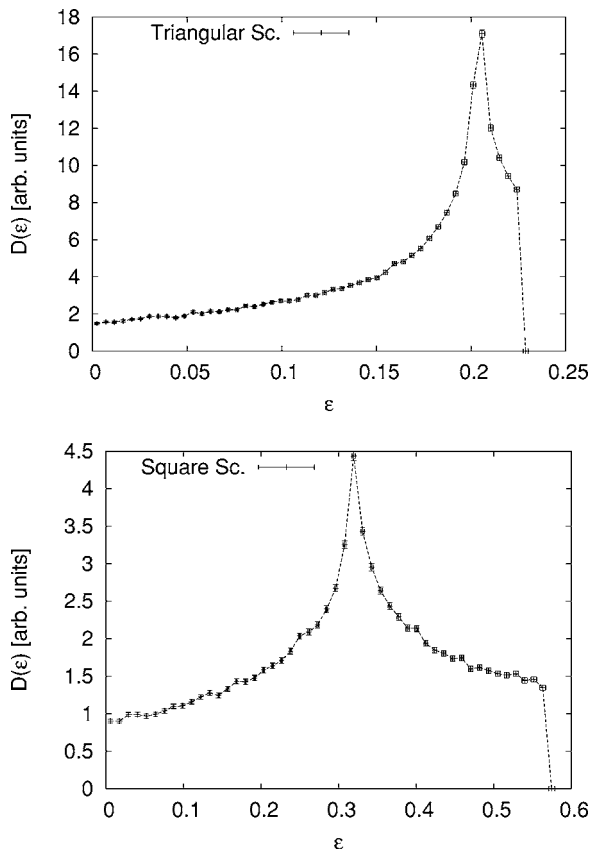
FIG. 11. DOS for a screened Fröhlich polaron with $R_{sc}=1$, $\lambda =8$, and $\bar{\omega}=8$. Again, the lattice dimensionality determines the presence of van Hove singularities. The Fröhlich polarons on both lattices are expected to have similar transport properties.

FIG. 12. Ratio of the effective bandwidth of the screened Fröhlich polaron on square and triangular lattices. $\lambda=1.4$ and $\bar{\omega} =1$. Note how the ratio of the bandwidths converges with increasing R_{sc}. This shows that the effects of lattice type are essentially washed out for long-range potentials.

technique. The effective mass, isotope coefficient, ground-state energy, phonon number, density of states, and polaron spectrum were calculated for the Holstein and Fröhlich polarons. Several lattices were investigated: linear, triangular, square, cubic, face-center cubic, hypercubic, hexagonal, and body-center cubic. The results were compared with analytic forms from weak- and strong-coupling perturbation theory.

The overriding factor for polaron dynamics in the Holstein model is found to be the number of nearest neighbors. For instance, the ground-state properties for the Holstein pola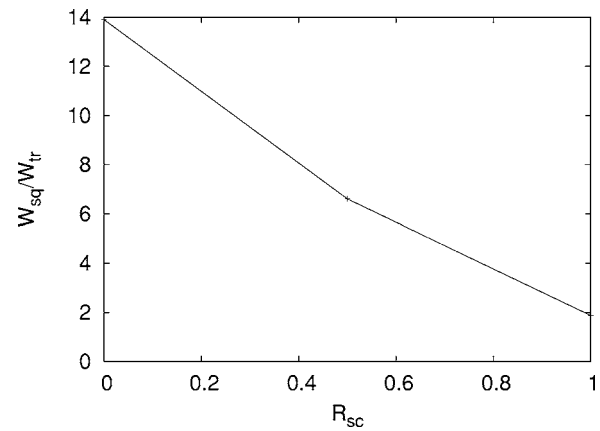ron on the triangular lattice ($z=6$) compare most closely with the cubic lattice ($z=6$) and not the square lattice (which might naïvely be expected since square and triangular lattices have the same dimensionality). Alternatively, when spectral properties such as the DOS and spectrum are considered, the lattice type is strongly responsible for the shape of the spectrum/DOS, but the band width is most closely related to the number of nearest neighbors. This is particularly obvious when the Lang-Firsov antiadiabatic limit is considered.

When an extended Fröhlich polaron is considered, the picture changes significantly. In that case, it is dimensionality which most strongly determines the form of the dynamic quantities (such as the effective mass), and not the number of nearest neighbors, since the lattice distortion surrounding the polaron is spread over a number of lattice sites. The bandwidths of the triangular and cubic lattices converge as the screening length is increased, even for moderate length scales of the potential.

[1] G. M. Zhao and D. E. Morris, Phys. Rev. B **51**, R16487 (1995); G.-M. Zhao, M. B. Hunt, H. Keller, and K. A. Müller, Nature (London) **385**, 236 (1997); R. Khasanov, D. G. Eshchenko, H. Luetkens, E. Morenzoni, T. Prokscha, A. Suter, N. Garifianov, M. Mali, J. Roos, K. Conder, and H. Keller, Phys. Rev. Lett. **92**, 057602 (2004).

[2] A. Lanzara, P. V. Bogdanov, X. J. Zhou, S. A. Kellar, D. L. Feng, E. D. Lu, T. Yoshida, H. Eisaki, A. Fujimori, K. Kishio, J. I. Shimoyana, T. Noda, S. Uchida, Z. Hussain, and Z. X. Shen, Nature (London) **412**, 510 (2001); G.-H. Gweon, T. Sasagawa, S. Y. Zhou, J. Craf, H. Takagi, D.-H. Lee, and A. Lanzara, *ibid.* **430**, 187 (2004).

[3] D. Mihailović, C. M. Foster, K. Voss, and A. J. Heeger, Phys. Rev. B **42**, 7989 (1990).

[4] P. Calvani, M. Capizzi, S. Lupi, P. Maselli, A. Paolone, P. Roy, S. W. Cheong, W. Sadowski, and E. Walker, Solid State Commun. **91**, 113 (1994).

[5] T. Egami, J. Low Temp. Phys. **105**, 791 (1996).

[6] G.-M. Zhao, K. Conder, H. Keller, and K. A. Müller, Nature (London) **381**, 676 (1996); A. S. Alexandrov, G.-M. Zhao, H. Keller, B. Lorenz, Y. S. Wang, and C. W. Chu, Phys. Rev. B **64**, 140404(R) (2001).

[7] A. S. Alexandrov, Phys. Rev. B **53**, 2863 (1996); Phys. Rev. Lett. **82**, 2620 (1999); A. S. Alexandrov and A. M. Bratkovsky, *ibid.* **84**, 2043 (2000).

[8] D. M. Edwards, Adv. Phys. **51**, 1259 (2002).

[9] A. S. Alexandrov and N. F. Mott, Rep. Prog. Phys. **57**, 1197 (1994); *Polarons and Bipolarons* (World Scientific, Singapore, 1995).

[10] J. T. Devreese, in *Encyclopedia of Applied Physics* (VCH Publishers, Berlin, 1996), Vol. 14, p. 383.

[11] A. B. Migdal, Zh. Eksp. Teor. Fiz. **34**, 1438 (1958) [Sov. Phys. JETP **7**, 996 (1958)].

[12] A. S. Alexandrov, V. N. Grebenev, and E. A. Mazur, Pis'ma Zh. Eksp. Teor. Fiz. **45**, 357 (1987) [JETP Lett. **45**, 455 (1987)].

[13] F. Dogan and F. Marsiglio, Phys. Rev. B **68**, 165102 (2003).

[14] J. P. Hague, J. Phys.: Condens. Matter **15**, 2535 (2003); **17**, 5663 (2005), and references therein.

[15] A. S. Alexandrov, *Theory of Superconductivity: From Weak to Strong Coupling* (IoP Publishing, Bristol, 2003).

[16] I. G. Lang and Yu. A. Firsov, Zh. Eksp. Teor. Fiz. **43**, 1843 (1962) [Sov. Phys. JETP **16**, 1301 (1963)].

[17] S. Ciuchi, F. de Pasquale, S. Fratini, and D. Feinberg, Phys. Rev. B **56**, 4494 (1997).

[18] A. S. Alexandrov, V. V. Kabanov, and D. K. Ray, Phys. Rev. B **49**, 9915 (1994); H. Fehske, H. Röder, G. Wellein, and A. Mistriotis, *ibid.* **51**, 16582 (1995); G. Wellein, H. Röder, and H. Fehske, *ibid.* **53**, 9666 (1996); F. Marsiglio, Physica C **244**, 21 (1995); W. Stephan, Phys. Rev. B **54**, 8981 (1996); M. Capone, W. Stephan, and M. Grilli, *ibid.* **56**, 4484 (1997).

[19] S. A. Trugman, J. Bonča, and L.-C. Ku, Int. J. Mod. Phys. B **15**, 2707 (2001); L.-C. Ku, S. A. Trugman, and J. Bonča, Phys. Rev. B **65**, 174306 (2002), and references therein.

[20] J. E. Hirsch and E. Fradkin, Phys. Rev. Lett. **49**, 402 (1982); Phys. Rev. B **27**, 4302 (1983); E. Fradkin and J. E. Hirsch, *ibid.* **27**, 1680 (1983).

[21] H. De Raedt and A. Lagendijk, Phys. Rev. Lett. **49**, 1522 (1982); Phys. Rev. B **27**, 6097 (1983); **30**, 1671 (1984); Phys. Rep.

[22] **127**, 234 (1985), and references therein.

[22] E. Jeckelmann and S. R. White, Phys. Rev. B **57**, 6376 (1998); E. Jeckelmann, C. Zhang, and S. R. White, *ibid.* **60**, 7950 (1999); C. Zhang, E. Jeckelmann, and S. R. White, *ibid.* **60**, 14092 (1999).

[23] P. E. Kornilovitch, Phys. Rev. Lett. **81**, 5382 (1998); Phys. Rev. B **60**, 3237 (1999).

[24] P. E. Spencer, J. H. Samson, P. E. Kornilovitch, and A. S. Alexandrov, Phys. Rev. B **71**, 184310 (2005).

[25] M. Hohenadler, D. Neuber, W. von der Linden, G. Wellein, J. Loos, and H. Fehske, Phys. Rev. B **71**, 245111 (2005).

[26] M. Hohenadler, H. G. Evertz, and W. von der Linden, Phys. Rev. B **69**, 024301 (2004).

[27] N. V. Prokof'ev and B. V. Svistunov, Phys. Rev. Lett. **81**, 2514 (1998); A. S. Mishchenko, N. V. Prokof'ev, A. Sakamoto, and B. V. Svistunov, Phys. Rev. B **62**, 6317 (2000).

[28] A. Macridin, G. A. Sawatzky, and M. Jarrell, Phys. Rev. B **69**, 245111 (2004).

[29] R. P. Feynman, Phys. Rev. **97**, 660 (1955); *Statistical Mechanics* (Benjamin, Reading, MA, 1972), Chap. 8.

[30] P. E. Kornilovitch and E. R. Pike, Phys. Rev. B **55**, R8634 (1997).

[31] A. S. Alexandrov and P. E. Kornilovitch, Phys. Rev. Lett. **82**, 807 (1999).

[32] P. E. Kornilovitch, Phys. Rev. B **59**, 13531 (1999).

[33] P. E. Kornilovitch and A. S. Alexandrov, Phys. Rev. B **70**, 224511 (2004).

[34] T. Holstein, Ann. Phys. (N.Y.) **8**, 325 (1959); **8**, 343 (1959).

[35] H. Fehske, J. Loos, and G. Wellein, Phys. Rev. B **61**, 8016 (2000).

[36] J. Bonča and S. A. Trugman, Phys. Rev. B **64**, 094507 (2001).

[37] A. S. Alexandrov, Phys. Rev. B **46**, R14932 (1992).

[38] H. Fröhlich, Adv. Phys. **3**, 325 (1954).

[39] V. V. Kabanov and O. Yu. Mashtakov, Phys. Rev. B **47**, 6060 (1993).